McGunnigle, J.P., et al., 2022, Triple oxygen isotope evidence for a hot Archean ocean: Geology, v. 50, https://doi.org/10.1130/G50230.1

SUPPLEMENTARY INFORMATION 1. SAMPLE DESCRIPTIONS

Hole 504B was a hole drilled into 5.9 Myr old crust approximately 200 km south of the Costa Rica Rift spreading center and is the deepest hole in the oceanic crust, penetrating a depth of 2,111 meters below seafloor (mbsf). The hole is drilled through 274.5 m of sediment, 571.5 m of volcanic rocks, a 209 m volcanic-dike transition zone, and 1056 m of a sheeted dike complex (Alt et al., 1996). Low temperature altered 504B samples analyzed in this study were recovered from the volcanic section of the crust. 504B is the most widely studied oceanic basement core because of the site's unique preservation of alteration phases that record the evolution of hydrothermal alteration systems. Previous oxygen isotope work on volcanic section 504B basalts show a range in $\delta^{18}O$ values from 5.8 to 12.0‰, with most samples falling within the range of 6.1 to 8.5‰ (Alt et al., 1986). All basalts recovered from 504B are tholeiitic and the alteration mineralogy of 504B has been well documented in Alt et al. (1985) and Alt et al. (1996). Propagation of the Cocos-Nazca spreading center westward toward the East Pacific Rise has produced the unique Hess Deep rift valley containing exposed lower crustal magmatic rocks and upper mantle peridotites, as well as upper crustal sheeted dikes and basalt flows. Located near the Pacific, Cocos, and Nazca triple junction, the Hess Deep rift valley was first cored during ODP expedition 147, and later during IDOP expedition 345. All Hess Deep samples analyzed from this study are from Expedition 345 Hole J. Drilling into Hole J was shallow and recovered ~ 26 m from Unit I: rubble, 29.8 m from Unit II: Oikocryst-Bearing Layered Gabbro Series, and 56 m from Unit III:

Troctolites for a total drill depth of 1111.8 mbsf. Samples analyzed in this study are from Unit II and Unit III.

The triple oxygen isotope composition of high temperature altered plutonic rocks and mineral separates from IODP Expedition 345 Hess Deep Core Hole J, low temperature altered basalts from DSDP Expeditions 70 and 83 Hole 504B and DSDP Expedition 51 Hole 417A, a chlorite mineral separate from the Mid-Atlantic Ridge, and experimentally altered basalts from Cole et al. (1987) were measured to examine basalt-water alteration trends and develop a mass balance model for the oceans. All natural oceanic basalt samples analyzed have been provided by the IODP Gulf Coast Repository, except samples 417A 32-4, 20-29, and HU-120-3 which are described in Muehlenbachs (1980) and Muehlenbachs and Clayton (1972). Experimental hydrothermally altered basalts have been described in Cole et al. (1987). The following sample descriptions only include samples from IODP expedition 345 Hess Deep and DSDP expedition 70 504B. The reader is referred to Cole et al. (1987) for experimental basalts, Muehlenbachs (1980) for 51A/417A 32-4, 20-29, Muehlenbachs (1972) for HU-120-3, and Hardman et al. (2021) for Roberts Victor eclogite sample descriptions and information. For information regarding samples 504B 83 74-3, 199-199, 504B 83 80-1, 32-34, 504B 83 82-1, 68-70, and 504B 83 95-1, 59-64 the reader is referred to Alt et al. (1996). 504B low temperature alteration phases have been identified using Alt et al. (1996) and Hess Deep high temperature alteration phases have been identified using Gillis et al. (2014) as references.

504B Sample Descriptions

504B 70 37-1 36-38

Sample 504B 70 37-1, 36-38 is an altered basalt comprised of ~ 30% Ca-rich plagioclase, 5% clinopyroxene, 5% orthopyroxene, and 60% alteration assemblages consisting mainly of saponite. Plagioclase occurs as tabular subhedral to euhedral grains, and clinopyroxene and orthopyroxene are anhedral to subhedral. Grain sizes range from fine to medium for plagioclase, and very fine to fine for clinopyroxene, orthopyroxene, and alteration assemblages. Saponite fully replaces clinopyroxene and orthopyroxene and partially replaces plagioclase ubiquitously throughout the sample. Partial replacement of plagioclase, clinopyroxene, and orthopyroxene by minor chlorite is common. Individual Fe-oxyhydroxide veins frequently cut orthopyroxene and clinopyroxene grains, and a single Fe-oxyhydroxide vein cuts through the entire sample.

504B 70 40-3 133-135

Sample 504B 70 40-3, 133-135 is an altered basalt comprised of ~ 45% Ca-rich plagioclase, 30% clinopyroxene, 10% orthopyroxene and 15% secondary assemblages consisting mainly of saponite. Plagioclase occurs as tabular anhedral to subhedral grains, and clinopyroxene and orthopyroxene are anhedral. Grain sizes range from fine to medium for plagioclase, and very fine to fine for clinopyroxene, orthopyroxene, and alteration assemblages. Fine Fe-oxyhydroxide rich halos occur sparsely in patches throughout the sample and often enclosing talc and chlorite, possibly indicating full replacement olivine. Replacement of plagioclase, pyroxene, and orthopyroxene by saponite and minor phillipsite and chlorite is ubiquitous and ranges from mild to intense. Saponite and minor celadonite also occurs in veins

cutting through all primary mineral assemblages. Pyrite is present intermittently throughout the sample and occurs as fine subhedral grains.

504B 70 48-3, 21-23

Sample 504B 70 48-3, 21-21 is an altered basalt comprised of ~ 40% Ca-rich plagioclase, 35% clinopyroxene, 10% orthopyroxene, and 15% alteration assemblages consisting mainly of zeolite. Plagioclase occurs as tabular anhedral grains, and clinopyroxene and orthopyroxene range from anhedral to subhedral. Grain sizes range from fine to medium for plagioclase, and very fine to fine for clinopyroxene, orthopyroxene, and alteration assemblages. Fibrous zeolite is ubiquitous throughout the sample and partially replaces all primary minerals. Intense to complete replacement of orthopyroxene and clinopyroxene by saponite, and minor replacement of all primary minerals by chlorite is common with pyroxene commonly exhibiting > 80% alteration. Partial replacement of plagioclase by celadonite is rare and fine, subhedral oxides are prevalent throughout the sample.

Hess Deep Sample Descriptions

345-U1415J-9R-1, 46-50

Sample 345-U1415J-9R-1, 46-50 is an altered olivine-bearing gabbro comprised of ~ 35% orthopyroxene, 25% clinopyroxene, 25% plagioclase, 10% olivine, and 5% alteration assemblages consisting mainly of serpentine, chlorite, prehnite, and amphibole. Orthopyroxene, clinopyroxene, and plagioclase are anhedral to subhedral and olivine is subhedral to euhedral. Orthopyroxene, clinopyroxene, and plagioclase grains are coarse to very coarse, and olivine grains are medium to

coarse. Orthopyroxene is mild to intensely altered by chlorite and amphibole, with some grains exhibiting near complete replacement by amphibole. Clinopyroxene is mildly replaced by serpentine, and plagioclase is moderately altered by prehnite and serpentine. Olivine alteration is variable, with some grains exhibiting complete replacement by serpentine and chlorite while some grains are mildly altered by serpentine.

345-U1415J-13R-1, 29-31

Sample 345-U1415J-13R-1, 29-31 is an altered troctolite comprised of ~ 50% Ca-rich plagioclase, 15% olivine, and 35% alteration assemblages consisting mainly of serpentine and unidentifiable clays. Plagioclase occurs as tabular anhedral to subhedral grains, and olivine is anhedral with rare skeletal grains. Grain sizes range from coarse to very course for plagioclase and olivine, and alteration assemblages are fine grained. Serpentine and unidentifiable clay minerals intensely to completely alter olivine, with olivine commonly exhibiting > 90% alteration. Plagioclase is significantly less altered than olivine but is commonly replaced by unidentifiable clays. Serpentine and chlorite veins commonly cut all minerals, and range in size from fine to medium and one medium chlorite veins cuts through the whole sample. Undulose extinction and fracturing are pervasive in plagioclase, indicating substantial sample deformation.

345-U1415J-13R-1, 53-57

Sample 345-U1415J-13R-1, 53-57 is an altered olivine-bearing gabbro comprised mainly of intensely altered plagioclase, olivine, clinopyroxene, and orthopyroxene, with alteration assemblages of prehnite, serpentine, and chlorite

constituting > 80% of the sample. Plagioclase and remnant olivine grains are coarse, clinopyroxene and orthopyroxene are medium to course, and alteration assemblages are medium to coarse grained. Plagioclase is intensely to completely altered by prehnite, and olivine is completely replaced by serpentine. Orthopyroxene and clinopyroxene are replaced by minor chlorite, minor amphibole, and unidentifiable clay minerals. Corona textures are prevalent and consist of aggregate, fine-grained tremolite and chlorite enclosing olivine and plagioclase and make up < 5% of the sample. Prehnite and chlorite veins are ubiquitous, with a single very coarse prehnite vein cut by smaller chlorite veins cutting through the whole sample.

345-U1415J-14G-1, 0-6

Sample 345-U1415J-14G-1, 0-6 is an altered troctolite consisting mainly of intensely altered plagioclase and olivine, with alteration assemblages of serpentine, prehnite, clinozoisite, epidote, chlorite, quartz, and unidentifiable clay minerals constituting > 80% of the sample. Plagioclase and remnant olivine are coarse, while alteration assemblages range in size from very fine (clays, clinozoisite) to fine (serpentine, prehnite, epidote). Plagioclase is mildly to moderately altered by prehnite, clinozoisite, epidote, and clays. Clinozoisite and epidote assemblages appear intergrown and to be replacing both plagioclase and prehnite. Olivine is completely replaced by serpentine and minor clay minerals, with chlorite and secondary quartz occurring adjacent with partially replaced olivine. Prehnite and serpentine veins are ubiquitous and cut both primary mineral grains throughout the whole sample.

345-U1415J-22G-1, 4-9

Sample 345 22-1, 4-9 is an altered gabbronorite comprised of ~ 55% orthopyroxene, 30% plagioclase, 5% clinopyroxene, and 10% alteration assemblages consisting mainly of serpentine, prehnite, chlorite, amphibole, and unidentifiable clay minerals. Orthopyroxene and plagioclase are anhedral and range in grain size from coarse to very coarse, and alteration assemblages are fine grained. Orthopyroxene and clinopyroxene are moderately to intensely altered by serpentine, chlorite, and minor amphibole, and plagioclase is mildly to moderately altered by prehnite and clays. Serpentine veins cut throughout the entirety of the sample and are often accompanied by small cross-cutting chlorite veins. Undulose extinction and fracturing are pervasive in orthopyroxene, indicating substantial sample deformation.

SUPPLEMENTARY INFORMATION 2. METHODS

Triple oxygen isotope measurements were made at the University of New Mexico's Center for Stable Isotopes (CSI) using the laser fluorination process of Sharp (1990), and the Ni "bomb" method similar to Clayton and Mayeda (1963). High temperature altered crust and mineral separate samples were loaded into a Ni sample block with 44 sample holes and sample sizes ranging from 1.5-3 mg. The sample chamber was evacuated with a turbomolecular pump for approximately 24 hours while heated with a halogen lamp to achieve high vacuum in the chamber and gas line prior to analysis. The UNM San Carlos Olivine standard was analyzed at the start of each day to ensure calibration of sample runs. The $\delta^{18}O$ and $\delta^{17}O$ values the UNM San Carlos olivine standard are 2.75 and 5.32‰ ($\Delta'^{17}O$ = -0.52, λ = 0.528), respectively, relative to VSMOW – SLAP2 (Sharp and Wostbrock, 2021). Uncertainties in the data are ±0.15 ‰ for $\delta^{18}O$ and 0.01‰ for $\Delta'^{17}O$. The sample chamber was then pre-fluorinated with 100 torr BrF_5 for 1 hour at room temperatures to react away any remaining water vapor or other contaminants from the samples.

High temperature altered crustal rocks were fluorinated using 100 torr BrF_5 and heated with a 50 W CO_2 laser until complete fluorination had occurred. In some instances, the sample chamber was kept at 0°C by placing a dewar filled with ice water under the chamber to minimize passive reaction that might occur when BrF_5 was introduced into the chamber. Based on San Carlos Olivine standardization analyses at room temperature and 0°C, no evidence was found for passive reaction occurring in Hess Deep gabbros and troctolites. After fluorination of a sample, excess BrF_5 and silicate fluorination byproducts were removed by cooling a trap

containing gasses with liquid nitrogen. To purify the liberated O_2, the gas was transferred through a trap cooled under liquid nitrogen conditions, followed by a NaCl trap heated to approximately 100°C, followed by a final cooled trap to remove any fluorination products. O_2 was subsequently transferred into a 5 Å mol sieve trap for absorption of O_2 under liquid nitrogen conditions. The sieve trap was then heated, and the sample gas was carried through a 13x mol sieve gas chromatography column in a purified He stream at a constant flow rate of 5.0 ml/min to remove any traces of NF_3. The sample was then collected in a second 5 Å mol sieve filled with zeolites cooled under liquid nitrogen conditions at the inlet of a Thermo-Finnegan MAT 253 dual-inlet isotope ratio mass spectrometer.

Analysis of reactive low temperature altered basalts were made using conventional fluorination using the “Ni bomb” method due to passive reaction that might occur when BrF_5 was introduced into the sample chamber during the laser fluorination process. For this method, samples were loaded into Ni tubes and heated at 100 °C for 1 hour to remove any water vapor from the samples and inside the tubes. 100 torr BrF_5 was then introduced into the tubes and the tubes were subsequently heated to 600 °C and reacted overnight. After full fluorination has occurred, the tubes were cooled using liquid nitrogen to remove remaining BrF_5 and residual fluorination products. The liberated O_2 was then released into the O_2 gas line and purified using the same procedure described above.

During mass spectrometer analyses, the intensities of both the sample and reference gas were matched with adjustments to bellow compression levels to obtain intensities between 3.0 – 4.0 volts for each sample run. The CSI reference

gas used for each analysis is calibrated relative to the VSMOW2-SLAP2 scale as described in Wostbrock et al. (2020). Oxygen isotopes were measured using long collection times of 26 seconds with 30 iterations occurring per analysis against the O_2 reference gas to achieve the desired high precision necessary to measure the triple oxygen isotopes of samples.

Prior to analysis, whole-rock samples were powdered in a steel mortar and pestle to ensure homogenization of highly heterogeneous rocks. Precipitate carbonate assemblages were separated from whole-rock samples by hand to eliminate CO_2 liberation during the fluorination process. CO_2 is estimated to only constitute 2.5% of the oceanic crust and is not a significant enough component to consider in the low temperature basalt alteration process within the mass balance model (Coogan and Gillis, 2013; Coogan and Dosso, 2015). Plagioclase and olivine were separated from sample 345 13-1, 53-57 for analysis using a Frantz Isodynamic Magnetic Separator and hand picking.

All triple oxygen isotope results are reported in per mil notation and relative to the VSMOW2 where:

$$\delta = \left(\frac{R_x}{R_{std}} - 1\right) \times 1000 \quad (1)$$

and

$$\delta' = 1000 \times \ln\left(\frac{\delta}{1000} + 1\right) \quad (2)$$

and R_x is the ratio of the heavy to light isotope of any sample x and R_{std} is the ratio of the heavy to light isotope of the standard (McKinney et al., 1950). To measure small deviations from a reference line (RL) used to approximate the terrestrial fractionation line (TFL), the $\Delta'^{17}O$ notation has been introduced and is defined as:

$$\Delta'^{17}O = \delta'^{17}O - \lambda_{RL} \times \delta'^{18}O + \gamma_{RL} \quad (3)$$

where λ_{RL} is the slope and γ_{RL} is the y-intercept of the reference fractionation line in $\delta'^{17}O$- $\delta'^{18}O$ space. This study uses the $\lambda_{RL} = 0.528$ convention and $\gamma_{RL} = 0$. For thermodynamic equilibrium fractionation processes between two phases, the slope λ can be replaced by θ to examine triple oxygen isotope fractionation trends where θ is defined by:

$$\theta_{A\text{-}B} = \frac{\delta'^{17}O_A - \delta'^{17}O_B}{\delta'^{18}O_A - \delta'^{18}O_B} \quad (4)$$

and A and B are any two phases in equilibrium.

The triple oxygen isotope equilibrium fractionation between two substances A and B with respect to ^{17}O and ^{18}O is given by:

$$\alpha^{17}O_{A\text{-}B} = (\alpha^{18}O_{A\text{-}B})^{\theta} \quad (5)$$

where $\alpha_{A\text{-}B} = R_A/R_B$ for any two phases A and B and θ is ~ 0.520 to 0.530. Like the equilibrium fractionation factor α, θ is a temperature dependent variable. Variations in θ with temperature are responsible for the mass dependent fractionation trends observed in triple oxygen isotope space.

SUPPLEMENTRY INFORMATION 3. DATA

All analyses made for altered oceanic crustal samples and mineral separates are reported here. If sample run values for $\delta^{18}O$ or $\Delta'^{17}O$ are beyond 3σ, the run was not included in the mean calculation. Sample 345-U1415J-13R-1, 53-57 appeared highly heterogenous with respect to alteration and was run using two different sections of the same sample. $\delta^{17}O$ and $\delta^{18}O$ values are reported to 3 significant figures to avoid rounding errors (Table S1-S4).

SUPPLEMENTARY INFORMATION 4. THE MASS BALANCE MODEL

Lithosphere-hydrosphere interactions that result in the net transfer of oxygen isotopes has been shown to buffer the oxygen isotope composition of the oceans to the modern steady state $\delta^{18}O$ value of 0 ± 2‰ (Muehlenbachs and Clayton, 1976; Muehlenbachs, 1998). Muehlenbachs and Clayton (1976) developed a mass balance model for the Earth's oceans using the $\delta^{18}O$ values of the analyzed altered basalts. In this model, four geologic processes are hypothesized to actively buffer the oxygen isotope composition of seawater: continental weathering, low temperature alteration of oceanic lithosphere, hydrothermal alteration of oceanic lithosphere, and water recycling – each of which contribute to the $\delta^{18}O$ value of seawater by functioning as a source or sink for the heavy oxygen isotope. Muehlenbachs (1998) later revised this model to incorporate the process of continental growth and adjust the high and low temperature basalt alteration parameters. The mass balance model is used to calculate the total oxygen isotope exchange resulting from hydrosphere-lithosphere interactions by considering the oxygen flux between reservoir and ocean and the isotopic fractionation between starting and altered reservoir. The result of the model indicates that if the considered processes operated the same way over a billion years, the equilibrium $\delta^{18}O$ value of the ocean should be approximately -0.1‰ (Muehlenbachs, 1998), a result lighter than the estimated $\delta^{18}O$ = -1‰ value of ice-free conditions (Shackleton and Kennett, 1975). Other box models considering oxygen isotope exchange processes occurring within the geological water cycle have found that early Earth oceans had a low $\delta^{18}O$ value that was progressively raised over time from changes in the ratio of high to low temperature alteration processes (Wallmann, 2001; Jaffres et al., 2007).

Sengupta and Pack (2018) presented a triple oxygen isotope mass balance model for the oceans adopted from the $\delta^{18}O$ model by Muehlenbachs (1998). The study measured the triple oxygen isotope composition of altered oceanic basalts, as well as a marine shale, and developed a model for both $\delta^{18}O$ and $\delta^{17}O$. Their results show a trend of decreasing $\delta^{18}O$ with increasing $\Delta'^{17}O$ as the high temperature altered crust flux ($\lambda_{basalt\text{-}water}$ = 0.5273) is reduced, and a trend of increasing $\delta^{18}O$ with decreasing $\Delta'^{17}O$ as the low temperature altered crust flux ($\lambda_{basalt\text{-}water}$ = 0.5247) is increased. The mass balance model shows that ice-free ocean conditions can be achieved with adjustments to the continental weathering and hydrothermal alteration fluxes. A predicted seawater evolution trend in $\delta'^{18}O$ – $\Delta'^{17}O$ space was modeled through high magnitude flux variations to examine if ancient marine chert data could be in equilibrium with a model predicted low $\delta^{18}O$ seawater composition. Translation of the triple oxygen isotope equilibrium fractionation curve for the SiO_2 – H_2O system determined in Sharp et al. (2016) to the model predicted low $\delta^{18}O$ seawater value suggest that Archean chert triple oxygen isotope data from Levin et al. (2014) could not be in equilibrium with a low $\delta^{18}O$ seawater and are best explained by diagenetic alteration.

The $\delta^{18}O$ mass balance model for the oceans originally developed in Muehlenbachs and Clayton (1976) revolutionized the stable isotope geochemistry community's understanding of the oxygen isotope composition of seawater. The subsequent models with the most substantial modifications come from Wallmann (2001) and Jaffres et al. (2007) who consider H_2O fluxes and ^{18}O transfer between reservoirs and was constructed assuming the ancient marine carbonate trend

reflects the evolution of seawater $\delta^{18}O$ to heavier values over time. The present study uses a method similar to Muehlenbachs (1998) but examines the solution for seawater $\delta^{18}O$ and $\Delta'^{17}O$ that would balance the contributions of each process (also the approach of Sengupta and Pack (2018)) as opposed to the net contributions each process has on the oxygen isotope composition of seawater. The distinction between the two different approaches is important because the assumptions and net results of running the model are different for both. Muehlenbachs (1998) assumes $\delta^{18}O = 0‰$ and the model can be used to examine the total contribution each process has on seawater $\delta^{18}O$ given this assumption. The approach used by Sengupta and Pack (2018) and this study does not assume seawater $\delta^{18}O = 0‰$ but that the oceans are in steady state and that a solution exists for seawater $\delta^{18}O$ and $\Delta'^{17}O$ that balances the contributions of each process.

Our model considers five geological processes that buffer the oxygen isotope composition of the oceans through hydrosphere-lithosphere interactions:

1. High temperature alteration of oceanic crust (*HT*)
2. Low temperature alteration of oceanic crust (*LT*)
3. Weathering of continents (*CW*)
4. Continental growth by sediment recycling (*CG*)
5. Mantle recycling of subducted water (*MR*)

The mass balance model calculates a seawater $\delta^{18}O$ and $\Delta'^{17}O$ that can balance the $\delta^{17}O$ and $\delta^{18}O$ contributions to the O isotope composition of seawater from each process and was run according to the following equations:

$$\frac{\partial}{\partial t}\delta^{18}O_{seawater} = 10^9 \text{ (yrs)} \times \sum \frac{F_i}{M_{ocean}} \times \Delta(\delta^{18}O_i) \quad (6)$$

and

$$\frac{\partial}{\partial t}\delta^{17}O_{seawater} = 10^9 \text{ (yrs)} \times \sum \frac{F_i}{M_{ocean}} \times \Delta(\delta^{17}O_i) \quad (7)$$

where F_i = the flux of buffering process *i* (g/yr) and M_{ocean} = the total mass of oxygen in the ocean (g). The model processes buffer the $\delta^{17}O$ and $\delta^{18}O$ values of seawater through seawater-rock interactions that result in a net oxygen isotope exchange and produce an altered lithospheric reservoir. The model reaches steady-state in 0.5 to 1.0×10^9 years. Sengupta and Pack (2018) found their model to reach steady state after 2.6×10^8 years, while Muehlenbachs (1998) found the model to reach steady state after 10^9 years. The Δ value quantifies the fractionation between unaltered and altered reservoir for each process where:

$$\Delta(\delta^{18}O_i) = \delta^{18}O_i^{unaltered} - \delta^{18}O_i^{altered} \quad (8)$$

and

$$\Delta(\delta^{17}O_i) = \delta^{17}O_i^{unaltered} - \delta^{17}O_i^{altered} \quad (9)$$

$\delta^{17}O$ and $\delta^{18}O$ values for altered and unaltered reservoirs are determined though measurements and estimations used to approximate the global averages for each reservoir. $\Delta'^{17}O$ measurements of altered oceanic crust from this study are used to determine $\delta^{17}O_{HT}^{altered}$ and $\delta^{17}O_{LT}^{altered}$, and all other reservoir $\delta^{17}O$ values are taken from Sharp et al. (2016), Bindeman et al. (2018), Sengupta and Pack (2018), and Cano et al. (2020). The five geological processes and triple oxygen isotope compositions of reservoirs in the model are considered as follows:

High temperature alteration of oceanic crust (*HT*) lowers the $\delta^{18}O$ and raises the $\Delta'^{17}O$ value of lithosphere from its unaltered $\delta^{18}O \approx 5.5 - 5.8‰$ and $\Delta'^{17}O \approx -0.057‰$

to an average altered $\delta^{18}O \approx 4.4‰$ from the migration of hot (estimated 300–500 °C) seawater through warm, newly formed oceanic lithosphere (Muehlenbachs, 1998; Sengupta and Pack, 2018; Cano et al., 2020). A corresponding altered reservoir $\Delta'^{17}O = -0.008‰$ ($\lambda = 0.528$) was determined by Sengupta and Pack (2018) based on high temperature altered DSDP/ODP hole 504B basalts. The triple oxygen isotope results from the present study for samples from IODP Hess Deep plutonic samples indicate a corresponding $\Delta'^{17}O = -0.05‰$, significantly different that the findings of Sengupta and Pack (2018). Hot seawater migration through the crust is estimated to affect up to 5 km of the oceanic lithosphere with F_{HT} being the largest in model by approximately a factor of two. Formation of low $\delta^{18}O$ and $\Delta'^{17}O$ greenstone alteration phases from high temperature fluid-rock interaction enriches the oceans in $\delta^{18}O$ and depletes the oceans in $\Delta'^{17}O$.

Low temperature alteration of oceanic crust (*LT*) results from the percolation of cold seawater through cooled, off-axis crust which raises the $\delta^{18}O$ and lowers the $\Delta'^{17}O$ of the unaltered oceanic lithosphere to an average $\delta^{18}O \approx 9.6‰$ (Muehlenbachs, 1998; Sengupta and Pack, 2018). Sengupta and Pack (2018) found the corresponding altered $\Delta'^{17}O = -0.098‰$ ($\lambda = 0.528$) based on low temperature altered IODP hole U1383C basalts. This study found a heavier corresponding *LT* $\Delta'^{17}O = -0.082‰$ based on measurements of DSDP hole 504B and hole 417A basalts. Percolation of cold seawater through the lithosphere is shallow and is estimated to affect only the upper 600 m of the crust and results in a low $F_{LT} \approx 1/9$ F_{HT}. Low temperature alteration of oceanic basalt forms hydrous clay minerals with large $\delta^{18}O$ and low $\Delta'^{17}O$ values and depletes the oceans in $\delta^{18}O$ and enriches the

oceans in $\Delta'^{17}O$. Fractionation between seawater and reservoir is a function of the reaction temperature and the oxygen isotope composition of the seawater and reservoir. Keeping the Δ equations as a function of seawater allows for examination of the contributions from each process with different seawater $\delta^{18}O$ and $\Delta'^{17}O$ compositions.

Weathering of continents (*CW*) results from interaction between continental lithosphere and low $\delta^{18}O$ meteoric water, raising the $\delta^{18}O$ and lowering the $\Delta'^{17}O$ of the continents. The flux estimate considers the present-day river sediment load containing 50% recycled sediment (not net $\delta^{18}O$ or $\Delta'^{17}O$ transfer), 25% weathered igneous crust, and 25% weathered metamorphic crust. The modeled process estimates a weathered crustal reservoir to be a shale with $\delta^{18}O$ = 17.1‰ and $\Delta'^{17}O$ = -0.050‰ formed from the weathering of igneous crust of $\delta^{18}O$ = 7‰ and $\Delta'^{17}O$ = -0.048‰ and metamorphic crust of $\delta^{18}O$ = 12‰ and $\Delta'^{17}O$ = -0.053‰ (Muehlenbachs, 1998; Bindeman et al., 2018; Sengupta and Pack, 2018). The F_{CW} estimate is large and ≈ 1/2 F_{HT} and results in the depletion of $\delta^{18}O$ and enrichment of $\Delta'^{17}O$ to the oceans.

Continental growth through sediment recycling (*CG*) results from subduction of oceanic lithosphere with a marine sediment layer with an average $\delta^{18}O$ = 26‰ and $\Delta'^{17}O$ = -0.097‰ into the mantle (Sharp et al., 2016). This model considers the subducting slab to be 90% basaltic crust and 10% ocean precipitated SiO_2 sediments with a small F_{CG} ≈ 1/12 F_{HT}. The average triple oxygen isotope composition of oceanic lithosphere was calculated using an unaltered reservoir $\delta^{18}O$ = 5.5‰ and $\Delta'^{17}O$ = -0.057‰ from Cano et al. (2020), average high and low

temperature altered oceanic lithosphere $\delta^{18}O_{HT}$ = 4.4‰ and $\delta^{18}O_{LT}$ = 9.6‰ values from Muehlenbachs (1998), and corresponding altered reservoir $\Delta'^{17}O_{HT}$ = -0.050‰ and $\Delta'^{17}O_{LT}$ = -0.082‰ determined in this study. Multiplying these values by their relative proportions from the flux equations yields an estimated average basaltic crust of $\delta^{18}O$ = 5.1‰ and $\Delta'^{17}O$ = -0.052‰. The mantle is estimated to have an average $\delta^{18}O$ = 5.6‰ and $\Delta'^{17}O$ = -0.060‰ (Cano et al., 2020). $\delta^{18}O$ depletion and $\Delta'^{17}O$ enrichment of the oceans is reflected in the high $\delta^{18}O$ and low $\Delta'^{17}O$ values of island arcs compared to intraplate derived volcanic crust, which is generated through the assimilation of chemical marine sediments into the mantle.

Mantle recycling of subducted water results from the subduction of chemically bound water in the altered oceanic crust, as well as water trapped in sediment pores, that equilibrates with the mantle and is volcanically outgassed at higher $\delta^{18}O$ and lower $\Delta'^{17}O$ values. Muehlenbachs (1998) estimated a 3‰ fractionation between oceanic lithosphere and chemically bound water which can be used to estimate recycled water $\delta^{18}O$. Using a θ = 0.528 between rock and water, the $\delta^{17}O$ of the water can also be estimated (Sengupta and Pack, 2018). The F_{MR} estimate is small and ≈ 0.04 F_{HT} and results in a minor enrichment of $\delta^{18}O$ and minor depletion of $\Delta'^{17}O$ to the oceans.

The steady state results of running the model can be seen in **Fig. S1**. While examining the effects of large increases or decreases in the budget-dominating *HT* and *CW* processes on seawater $\delta^{18}O$ and $\Delta'^{17}O$, it was found that large increases and decreases in either flux result in no net change in seawater $\delta^{18}O$ or $\Delta'^{17}O$ because the model has reached a steady state condition. That is, increasing F_{CW} by

100x results in the same seawater $\delta^{18}O$ and $\Delta'^{17}O$ as increasing F_{CW} by 1000x. The sensitivity of the model to changes in $\Delta'^{17}O$ values for the altered *CW* reservoir was examined to account for uncertainties in $\Delta'^{17}O$ measurements and estimates. Sensitivity tests varying the shale $\Delta'^{17}O$ = -0.050‰ by ± 0.01‰ are shown in **Fig. S2**. Using a shale with $\Delta'^{17}O$ = -0.060‰ decreases the λ from λ = 0.524 to λ = 0.523 for the decreasing F_{HT} seawater evolution and results in a maximum $\Delta'^{17}O$ = 0.019 at F_{HT} = 0, a very minor $\Delta'^{17}O$ increase from the original $\Delta'^{17}O$ = 0.014 (**Fig. S2a**). Similarly, a shale with $\Delta'^{17}O$ = -0.040‰ results in a minor increase in λ to λ=0.525 and a seawater $\Delta'^{17}O$ = 0.011 at F_{HT} = 0. Using a shale with $\Delta'^{17}O$ = -0.060‰ results in a F_{CW} increasing seawater evolution trend with λ = 0.526 and F_{CW} × 100 seawater $\Delta'^{17}O$ = 0.019, a small decrease in λ and moderate increase in seawater $\Delta'^{17}O$ from the original trend (**Fig. S2b**). A shale with $\Delta'^{17}O$ = -0.040‰ results in effectively no change in λ and results in minor decrease in seawater $\Delta'^{17}O$ = 0.000‰ at F_{CW} × 100. Reduction of F_{MR} to a significantly lower value has been proposed by Miller et al. (2020) using seismic anisotropy measurements of the Middle America Trench. Running the model with F_{MR} from Miller et al. (2021) reduces F_{MR} by ~ 77%, effectively shutting off *MR*, and can bring the modeled seawater to a mean $\delta^{18}O$ = -0.37‰ with an unchanged $\Delta'^{17}O$ = -0.002. These calculations imply that if most bound and connate lithospheric water is discharged prior to subduction, the model comes into better agreement with the $\delta^{18}O$ ice-free estimate by only ~ -0.08‰.

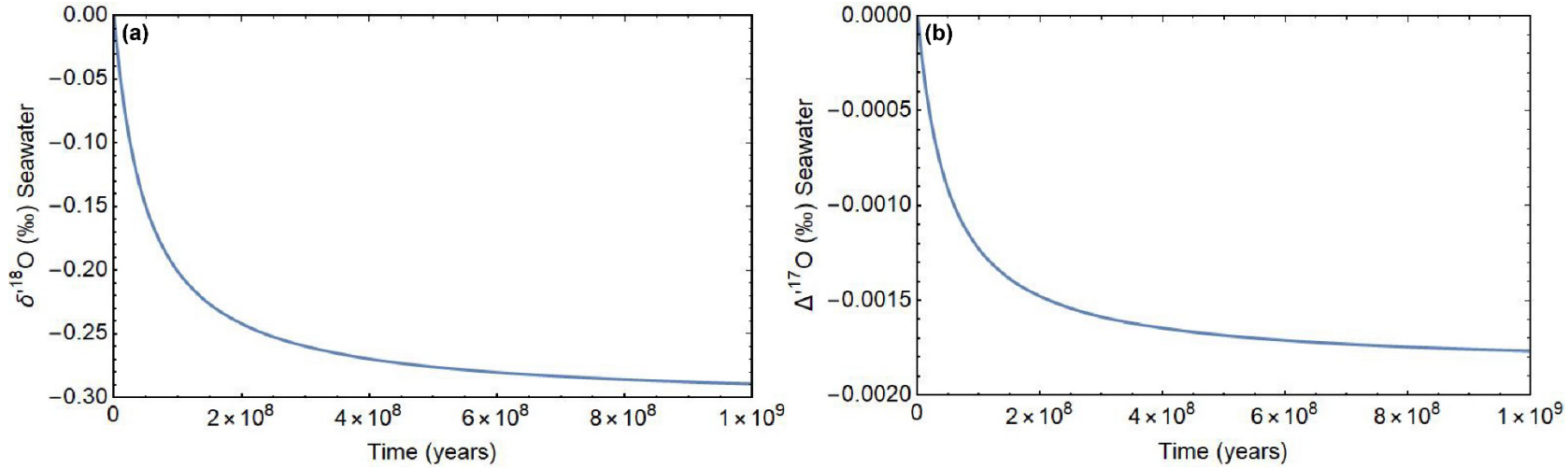

Fig. S1. Model variation in seawater $\delta^{18}O$ and $\Delta'^{17}O$ over time. (a) shows variation in seawater $\delta^{18}O$ over time. The model initially generates a seawater composition with $\delta^{18}O \approx 0‰$ and evolves to lighter values overtime with steady state reached at ~ (0.5 to 1) x 10^9 years with $\delta^{18}O \approx -0.29‰$. **(b)** shows variation in seawater $\Delta'^{17}O$ over time. The model generates a seawater $\Delta'^{17}O \approx 0.000‰$ at time zero and evolves to a lighter $\Delta'^{17}O = -0.002‰$ over ~ (0.5 to 1) x 10^9 years as steady state is reached.

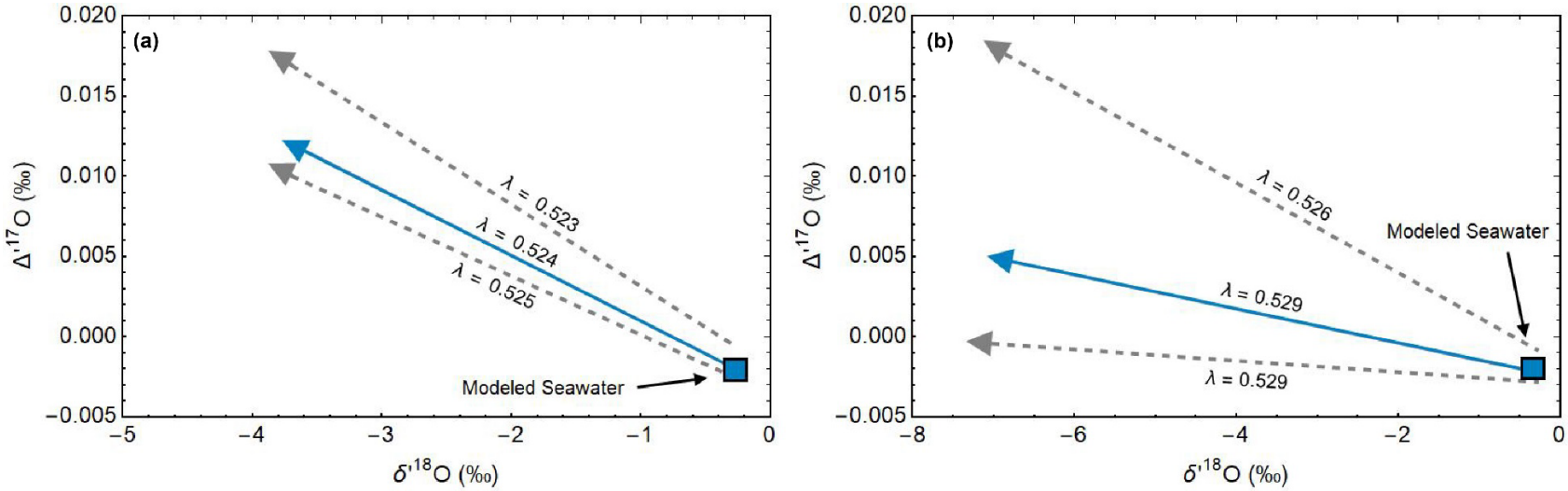

Fig. S2. Sensitivity tests of F_{HT} × 0 and F_{CW} × 100 seawater evolution trends. (a) shows changes in slope λ and seawater compositions for F_{HT} × 0 as *CW* shale endmember is varied between standard modeled $\Delta'^{17}O$ = -0.050‰ to $\Delta'^{17}O$ = -0.060‰ (λ = 0.523) and $\Delta'^{17}O$ = -0.040‰ (λ = 0.525). With λ = 0.523, seawater can evolve to a maximum $\Delta'^{17}O$ = 0.019 and with λ = 0.523 seawater evolves to a maximum $\Delta'^{17}O$ = 0.011‰. **(b)** shows changes in λ and seawater compositions for F_{CW} × 100 as the shale $\Delta'^{17}O$ varies. With λ = 0.526, seawater can evolve to a maximum $\Delta'^{17}O$ = 0.019 and with λ = 0.529 seawater can evolve to a maximum $\Delta'^{17}O$ = 0.000‰.

SUPPLEMENTARY INFORMATION 5. DIAGENETIC ALTERATION MODELLING

Diagenetic fluid modelling was examined according to the following equation after Taylor (1978):

$$\delta^{x}O_{final\ rock} = \frac{1000X + \alpha(X \times \delta^{x}O_{initial\ rock} - X \times \delta^{x}O_{initial\ water} - \delta^{x}O_{initial\ rock} - 1000X)}{\alpha X - \alpha - X} \quad (10)$$

where $\delta^{x}O$ is the delta composition for oxygen of atomic mass x, X is the F/R ratio, and α if the fractionation factor between the rock and water for ^{x}O. α values for SiO_2 – H_2O were calculated from Sharp et al. (2016) and vary for each alteration temperature. All samples from Lowe et al. (2020), Sengupta et al. (2020), and all but 3 samples from Liljestrand (2020) can be explained by a precipitation with our modeled F_{HT} × 0 seawater composition with an initial rock of $\delta^{18}O$ = 26.0‰ and $\Delta'^{17}O$ = -0.096‰, corresponding to an ocean temperature of 50°C (Lowe et al., 2020). Fluids with compositions ranging from $\delta^{18}O$ = -7 to -20‰ and $\Delta'^{17}O$ = 0.03 to 0.04‰ and alteration temperatures ranging from 50 to 200°C are required to explain the chert compositions. Samples from Liljestrand et al. (2020) generally require lighter $\delta^{18}O$ fluids and higher alteration temperatures than Lowe et al. (2020) and Sengupta et al. (2020), likely due to a higher degree of diagenetic alteration as suggested by Lowe et al. (2020). It is important to recognize that in nearly all samples a calculated F/R ratio using a given alteration temperature and fluid composition is not unique and multiple solutions exist to account for each sample $\delta^{18}O$ and $\Delta'^{17}O$ value. For a given sample suite, the solution alteration temperatures and diagenetic fluid composition that best fits the data is typically used. In Fig. 3, each study presents data from different sample suites and in the cases of Sengupta et al. (2020) and Liljestrand et al. (2020) there are multiple sample suites within the

data set and finding a best fit for fluid composition and alteration temperature that matches all data presented is unattainable.

Table S1: Roberts Victor eclogite sample analysis (all data relative to VSMOW)

Sample	$\delta^{17}O$ (‰)	$\delta^{18}O$ (‰)	$\delta'^{17}O$ (‰)	$\delta'^{18}O$ (‰)	$\Delta'^{17}O$ (‰)
RV-1GT	1.351	2.673	1.350	2.669	-0.059
	1.289	2.545	1.288	2.542	-0.054
Mean	1.320	2.609	1.319	2.606	-0.057
RV-1CPX	1.179	2.324	1.178	2.321	-0.047
RV-10GT	1.571	3.077	1.570	3.072	-0.052
	1.512	2.953	1.511	2.949	-0.046
Mean	1.542	3.015	1.540	3.010	-0.049
RV-10CPX	1.380	2.682	1.379	2.678	-0.035
RV-22GT	0.840	1.678	0.840	1.677	-0.046
	0.829	1.668	0.829	1.667	-0.051
Mean	0.835	1.673	0.834	1.672	-0.048
RV-22CPX	0.704	1.445	0.704	1.444	-0.059
	0.827	1.683	0.827	1.682	-0.061
Mean	0.766	1.564	0.765	1.563	-0.060
RV-20GT	1.394	2.724	1.393	2.720	-0.043
	1.383	2.725	1.382	2.721	-0.055
Mean	1.389	2.725	1.388	2.721	-0.049
RV-16GT	3.924	7.566	3.916	7.538	-0.063
	3.826	7.376	3.819	7.349	-0.062
Mean	3.875	7.471	3.868	7.443	-0.063
RV-16CPX	3.578	6.914	3.572	6.890	-0.066
RV-19GT	2.669	5.149	2.665	5.136	-0.046
	2.997	5.764	2.993	5.747	-0.042
Mean	2.833	5.457	2.829	5.442	-0.044
RV-19CPX	2.511	4.843	2.508	4.831	-0.043
RV-24GT-14	3.951	7.594	3.943	7.565	-0.051
	3.872	7.465	3.865	7.437	-0.062
Mean	3.912	7.530	3.904	7.501	-0.057
RV-24CPX	3.782	7.320	3.775	7.293	-0.076

RV-27GT	2.350	4.560	2.347	4.550	-0.055
	2.353	4.564	2.350	4.554	-0.054
Mean					
RV-27CPX	2.250	4.380	2.247	4.370	-0.060
	2.177	4.241	2.175	4.232	-0.060
Mean	2.214	4.311	2.211	4.301	-0.060

Note: Sample measurements reported in per mil notation relative to VSMOW2.GT designates a garnet mineral separate, and CPX designates a clinopyroxene separate.

Table S2: High temperature altered oceanic crust sample runs

Sample	$\delta^{17}O$ (‰)	$\delta^{18}O$ (‰)	$\delta'^{17}O$ (‰)	$\delta'^{18}O$ (‰)	$\Delta'^{17}O$ (‰)
345-U1415J-9R-1, 46-50	3.147	6.078	3.142	6.059	-0.057
	3.107	6.009	3.102	5.991	-0.061
	3.081	5.691	3.076	5.675	0.080
	2.863	5.558	2.859	5.543	-0.068
	3.010	5.819	3.005	5.802	-0.058
	2.963	5.774	2.958	5.757	-0.081
	2.442	4.746	2.439	4.735	-0.061
	2.448	4.740	2.445	4.729	-0.052
	2.520	4.878	2.517	4.866	-0.052
	2.563	4.988	2.560	4.976	-0.067
	2.777	5.369	2.773	5.355	-0.054
Mean	2.784	5.396	2.780	5.381	-0.061
345-U1415J-13R-1, 29-31	1.967	3.843	1.965	3.836	-0.060
	1.933	3.737	1.931	3.730	-0.038
	2.061	4.017	2.059	4.009	-0.058
	2.102	4.092	2.100	4.084	-0.056
	2.122	4.126	2.120	4.117	-0.054
	1.294	2.568	1.293	2.565	-0.061
	1.501	2.922	1.500	2.918	-0.041
	1.667	3.187	1.666	3.182	-0.014
	1.690	3.291	1.689	3.286	-0.046
Mean	1.834	3.575	1.832	3.568	-0.052
345-U1415J-13R-1, 53-57 (1)	2.569	4.982	2.566	4.970	-0.058
	2.395	4.651	2.392	4.640	-0.058
	2.204	4.263	2.202	4.254	-0.045
	2.369	4.582	2.366	4.572	-0.048
Mean	2.384	4.620	2.381	4.609	-0.052
345-U1415J-13R-1, 53-57 (2)	1.336	2.645	1.336	2.641	-0.059
	1.400	2.743	1.399	2.740	-0.048
	1.366	2.691	1.365	2.687	-0.054
	1.484	2.826	1.483	2.822	-0.007
	1.497	2.928	1.496	2.924	-0.048
	1.494	2.918	1.493	2.914	-0.045
	1.329	2.619	1.328	2.616	-0.053
	1.342	2.610	1.341	2.607	-0.035
Mean	1.395	2.736	1.394	2.733	-0.049
345-U1415J-22G-1, 4-8	2.607	5.073	2.603	5.060	-0.048

	2.561	4.998	2.558	4.986	-0.055
	2.481	4.825	2.478	4.814	-0.044
	2.619	5.049	2.616	5.036	-0.043
	2.562	4.957	2.559	4.945	-0.052
	2.278	4.412	2.275	4.402	-0.049
Mean	2.518	4.886	2.515	4.874	-0.049
345-U1415J-14G-1, 0-6	1.057	2.062	1.056	2.060	-0.031
	1.222	2.393	1.221	2.390	-0.041
	0.331	0.714	0.331	0.714	-0.046
	0.912	1.825	0.912	1.823	-0.051
	0.827	1.667	0.827	1.666	-0.053
	0.897	1.773	0.897	1.771	-0.039
Mean	0.983	1.944	0.983	1.942	-0.043

Note: Sample measurements reported in per mil notation relative to VSMOW2

Table S3: High temperature altered oceanic crust mineral separate sample runs

Sample	$\delta^{17}O$ (‰)	$\delta^{18}O$ (‰)	$\delta'^{17}O$ (‰)	$\delta'^{18}O$ (‰)	$\Delta'^{17}O$ (‰)
345-U1415J-13R-1, 53-57 (Olivine)	2.295	4.463	2.292	4.453	-0.059
	2.411	4.668	2.408	4.657	-0.051
	2.317	4.535	2.314	4.525	-0.075
	2.143	4.134	2.141	4.125	-0.038
Mean	2.292	4.450	2.289	4.440	-0.056
345-U1415J-13R-1, 53-57 (Plagioclase)	2.924	5.652	2.920	5.636	-0.056
	3.192	6.155	3.187	6.136	-0.053
	2.971	5.700	2.967	5.684	-0.034
	2.518	4.875	2.515	4.863	-0.053
	2.446	4.690	2.443	4.679	-0.028
Mean	2.901	5.596	2.897	5.580	-0.049
345-U1415J-13R-1, 53-57 (Prehnite)	0.998	1.988	0.998	1.986	-0.051
	0.825	1.639	0.825	1.638	-0.040
	0.799	1.601	0.799	1.600	-0.046
	0.854	1.692	0.854	1.691	-0.039
Mean	0.869	1.730	0.869	1.728	-0.044
HU-120-3 (Chlorite)	0.530	1.044	0.530	1.043	-0.021
	0.547	1.059	0.547	1.058	-0.012
	0.448	0.905	0.448	0.904	-0.030
Mean	0.508	1.002	0.508	1.002	-0.021

Note: Sample measurements reported in per mil notation relative to VSMOW2

Table S4: Low temperature altered oceanic crust sample runs

Sample	$\delta^{17}O$ (‰)	$\delta^{18}O$ (‰)	$\delta'^{17}O$ (‰)	$\delta'^{18}O$ (‰)	$\Delta'^{17}O$ (‰)
504B 70 37-1, 36-38	4.809	9.255	4.797	9.213	-0.067
	4.873	9.371	4.861	9.327	-0.064
	4.781	9.208	4.769	9.166	-0.070
Mean	4.821	9.278	4.809	9.235	-0.067
504B 70 40-3, 133-135	4.027	7.713	4.019	7.683	-0.038
	3.853	7.388	3.845	7.361	-0.041
	3.883	7.459	3.875	7.431	-0.048
	4.295	8.261	4.286	8.227	-0.058
Mean	4.014	7.705	4.006	7.676	-0.046
504B 70 48-3, 21-23	4.308	8.309	4.299	8.275	-0.070
	3.980	7.643	3.972	7.614	-0.049
	4.093	7.872	4.084	7.841	-0.056
	4.102	7.912	4.093	7.881	-0.068
Mean	4.121	7.934	4.112	7.903	-0.061
504B 83 74-3 199-199	3.216	6.182	3.211	6.163	-0.043
	3.229	6.261	3.224	6.241	-0.072
Mean	3.223	6.222	3.217	6.202	-0.057
504B 83 80-1 32-34	3.111	6.010	3.106	5.992	-0.057
504B 83 82-1 68-70	3.139	6.079	3.134	6.061	-0.066
	3.332	6.463	3.326	6.442	-0.075
Mean	3.236	6.271	3.230	6.251	-0.070
504B 83 95-1, 59-64	3.776	7.260	3.769	7.234	-0.051
	3.662	7.035	3.655	7.010	-0.046
Mean	3.719	7.148	3.712	7.122	-0.048
51A/417A 32-4, 20-29	7.626	14.704	7.597	14.596	-0.110
	7.256	13.976	7.230	13.879	-0.098
	7.483	14.398	7.455	14.296	-0.093
Mean	7.455	14.359	7.427	14.257	-0.100

Note: Sample measurements reported in per mil notation relative to VSMOW2

Table S5: Experimental hydrothermal altered oceanic basalt sample runs

Sample	$\delta^{17}O$ (‰)	$\delta^{18}O$ (‰)	$\delta'^{17}O$ (‰)	$\delta'^{18}O$ (‰)	$\Delta'^{17}O$ (‰)
1A (300°C)	2.336	4.534	2.333	4.524	-0.055
	2.447	4.744	2.444	4.733	-0.055
	2.239	4.320	2.236	4.311	-0.040
	2.305	4.427	2.302	4.417	-0.030
	2.079	4.039	2.077	4.031	-0.051
Mean	2.162	4.204	2.160	4.195	-0.055
2A (400°C)	1.624	3.180	1.623	3.175	-0.054
	1.638	3.170	1.637	3.165	-0.034
	1.674	3.225	1.673	3.220	-0.027
	1.498	2.984	1.497	2.980	-0.076
	1.716	3.324	1.715	3.318	-0.038
	1.502	2.955	1.501	2.951	-0.057
Mean	1.631	3.171	1.629	3.166	-0.042
2C (400°C)	1.537	2.975	1.536	2.971	-0.033
	1.552	2.985	1.551	2.981	-0.023
	1.634	3.120	1.633	3.115	-0.012
	1.719	3.295	1.718	3.290	-0.019
	1.550	3.035	1.549	3.030	-0.051
	1.560	3.039	1.559	3.034	-0.043
Mean	1.584	3.066	1.582	3.061	-0.034
2F (400°C)	1.808	3.492	1.806	3.486	-0.034
	1.917	3.720	1.915	3.713	-0.045
	1.881	3.648	1.879	3.641	-0.043
	1.830	3.525	1.828	3.519	-0.030
	1.682	3.290	1.681	3.285	-0.054
	1.876	3.685	1.874	3.678	-0.068
Mean	1.832	3.560	1.831	3.554	-0.046
6A (500°C)	1.043	2.069	1.042	2.067	-0.049
	1.106	2.144	1.105	2.142	-0.025
	1.186	2.293	1.185	2.290	-0.024
	1.068	2.050	1.067	2.048	-0.014
	0.872	1.705	0.872	1.704	-0.028
	0.856	1.724	0.856	1.723	-0.054
Mean	1.013	1.987	1.012	1.985	-0.036
3D(500°C)	0.453	0.924	0.453	0.924	-0.035
	0.733	1.425	0.733	1.424	-0.019
	0.596	1.181	0.596	1.180	-0.027

	0.468	0.899	0.468	0.899	-0.007
	0.710	1.400	0.710	1.399	-0.029
	0.704	1.428	0.704	1.427	-0.050
Mean	0.611	1.210	0.610	1.209	-0.028

Note: Sample measurements reported in per mil notation relative to VSMOW2

Table S6. Mass balance model fluxes and Δ equations for each seawater buffering process.			
Process	**Flux (g/yr)**	**$\Delta\delta^{17}O$(‰)**	**$\Delta\delta^{18}O$(‰)**
High Temperature Alteration (F_{HT})	1.87×10^{16}	$(2.8 - (\delta^{18}O_{SW} + 2.3))$	$(5.5 - (\delta^{18}O_{SW} + 4.4))$
Low Temperature Alteration (F_{LT})	2.2×10^{15}	$(2.8 - (\delta^{18}O_{SW} + 5.0))$	$(5.5 - (\delta^{18}O_{SW} + 9.6))$
Continental Weathering (F_{CW})	1.02×10^{16}	$-(0.125 \times (5.4 + \delta^{18}O_{SW}) + 0.125 \times (2.8 + \delta^{18}O_{SW}))$	$-(0.125 \times (10.2 + \delta^{18}O_{SW}) + 0.125 \times (5.2 + \delta^{18}O_{SW}))$
Continental Growth (F_{CG})	1.50×10^{15}	$2.9 - ((0.9 \times 2.6) + 0.1 \times (13.5 + \delta^{18}O_{SW}))$	$5.6 - ((0.9 \times 5.1) + 0.1 \times (26.0 + \delta^{18}O_{SW}))$
Mantle Recycling (F_{MR})	0.80×10^{15}	$2.9 - (\delta^{18}O_{SW} + 1.1)$	$5.6 - (\delta^{18}O_{SW} + 2.1)$

Supplementary References

Alt, J. C. *et al.* Hydrothermal alteration of a section of upper oceanic crust in the Eastern equatorial pacific: A synthesis of results from site 504 (DSDP legs 69, 70, and 83, and ODP legs 111, 137, 140, and 148). in *Proceedings of the Ocean Drilling Program, 148 Scientific Results* (Ocean Drilling Program, 1996).

Alt, J. C., Laverne, C. & Muehlenbachs, K. Alteration of the upper oceanic crust: Mineralogy and processes in deep sea drilling project hole 504B, leg 83. in *Initial Reports of the Deep Sea Drilling Project* (U.S. Government Printing Office, 1985).

Alt, J. C., Muehlenbachs, K. & Honnorez, J. An oxygen isotopic profile through the upper kilometer of the oceanic crust, DSDP Hole 504B. *Earth Planet. Sci. Lett.* **80**, 217–229 (1986).

Bindeman, I. N. *et al.* Rapid emergence of subaerial landmasses and onset of a modern hydrologic cycle 2.5 billion years ago. *Nature* **557**, 545–548 (2018).

Cano, E. J., Sharp, Z. D. & Shearer, C. K. Distinct oxygen isotope compositions of the Earth and Moon. *Nat. Geosci.* **13**, 270–274 (2020).

Clayton, R. N. & Mayeda, T. K. The use of bromine pentafluoride in the extraction of oxygen from oxides and silicates for isotopic analysis. *Geochim. Cosmochim. Acta* **27**, 43–52 (1963).

Coogan, L. A. & Dosso, S. E. Alteration of ocean crust provides a strong temperature dependent feedback on the geological carbon cycle and is a primary driver of the Sr-isotopic composition of seawater. *Earth Planet. Sci. Lett.* **415**, 38–46 (2015).

Coogan, L. A. & Gillis, K. M. Evidence that low-temperature oceanic hydrothermal systems play an important role in the silicate-carbonate weathering cycle and long-term climate regulation: OCEANIC HYDROTHERMAL CARBONATE UPTAKE. *Geochem. Geophys. Geosyst.* **14**, 1771–1786 (2013).

Jaffrés, J. B. D., Shields, G. A. & Wallmann, K. The oxygen isotope evolution of seawater: A critical review of a long-standing controversy and an improved geological water cycle model for the past 3.4 billion years. *Earth Sci. Rev.* **83**, 83–122 (2007).

Johnson, B. W. & Wing, B. A. Limited Archaean continental emergence reflected in an early Archaean ^{18}O-enriched ocean. *Nat. Geosci.* **13**, 243–248 (2020).

Levin, N. E., Raub, T. D., Dauphas, N. & Eiler, J. M. Triple oxygen isotope variations in sedimentary rocks. *Geochim. Cosmochim. Acta* **139**, 173–189 (2014).

Liljestrand, F. L. *et al.* The triple oxygen isotope composition of Precambrian chert. *Earth Planet. Sci. Lett.* **537**, 116167 (2020).

Lowe, D. R., Ibarra, D. E., Drabon, N. & Chamberlain, C. P. Constraints on surface temperature 3.4 billion years ago based on triple oxygen isotopes of cherts from the Barberton Greenstone Belt, South Africa, and the problem of sample selection. *Am. J. Sci.* **320**, 790–814 (2020).

McKinney, C. R., McCrea, J. M., Epstein, S., Allen, H. A. & Urey, H. C. Improvements in mass spectrometers for the measurement of small differences in isotope abundance ratios. *Rev. Sci. Instrum.* **21**, 724–730 (1950).

Muehlenbachs, K. The alteration and aging of the basaltic layer of sea floor: Oxygen isotope evidence from DSDP/IPOD legs 51, 52, and 53. in *Initial Reports of the Deep Sea Drilling Project* (U.S. Government Printing Office, 1980).

Muehlenbachs, K. The oxygen isotopic composition of the oceans, sediments, and the seafloor. *Chem. Geol.* **145**, 263-273 (1998).

Muehlenbachs, K. & Clayton, R. N. Oxygen isotope composition of the oceanic crust and its bearing on seawater. *J. Geophys. Res.* **81**, 4365–4369 (1976).

Muehlenbachs, K. & Clayton, R. N. Oxygen isotope geochemistry of submarine greenstones. *Can. J. Earth Sci.* **9**, 471–478 (1972).

Sengupta, S. & Pack, A. Triple oxygen isotope mass balance for the Earth's oceans with application to Archean cherts. *Chem. Geol.* **495**, 18–26 (2018).

Sengupta, S., Peters, S. T. M., Reitner, J., Duda, J.-P. & Pack, A. Triple oxygen isotopes of cherts through time. *Chem. Geol.* **554**, 119789 (2020).

Shackleton, N. J. & Kennett, J. P. Paleotemperature history of the Cenozoic and the initiation of antarctic glaciation: Oxygen and carbon isotope analyses in DSDP sites 277, 279 and 281. in *Initial Reports of the Deep Sea Drilling Project* (1975).

Sharp, Z. D. A laser-based microanalytical method for the in situ determination of oxygen isotope ratios of silicates and oxides. *Geochim. Cosmochim. Acta* **54**, 1353–1357 (1990).

Sharp, Z. D. *et al.* A calibration of the triple oxygen isotope fractionation in the SiO2–H2O system and applications to natural samples. *Geochim. Cosmochim. Acta* **186**, 105–119 (2016).

Taylor, H. P., Jr. Oxygen and hydrogen isotope studies of plutonic granitic rocks. *Earth Planet. Sci. Lett.* **38**, 177–210 (1978).

Wallmann, K. The geological water cycle and the evolution of marine $\delta^{18}O$ values. *Geochim. Cosmochim. Acta* **65**, 2469–2485 (2001).

Wostbrock, J. A. G., Cano, E. J. & Sharp, Z. D. An internally consistent triple oxygen isotope calibration of standards for silicates, carbonates and air relative to VSMOW2 and SLAP2. *Chem. Geol.* **533**, 119432 (2020).

Wostbrock, J.A.G. & Sharp, Z.D. Triple Oxygen Isotopes in Silica–Water and Carbonate–Water Systems. *Reviews in Mineralogy and Geochemistry* **86**, 367–400 (2021).